

© 2025 The Author(s)



Spatio-temporal changes of thermohaline properties and nutrients in the Mediterranean Sea

Ivona Siber, Frano Matić

University of Split, University Department of Marine Studies, Split, Croatia

Correspondence to:

Ivona Siber University of Split, University Department of Marine Studies Ulica Ruđera Boškovića 37, 21000 Split, Croatia ivona.siber18@gmail.com

Cite as

Siber I, Matić F. Spatio-temporal changes of thermohaline properties and nutrients in the Mediterranean Sea. ST-OPEN. 2025;6:e2025. 2415.11.

DOI:

https://doi.org/10.48188/so.6.13

Aim: To analyze long-term mean monthly values for sea surface height (SSH) and nutrient concentrations (ammonia, nitrate, phosphate, and chlorophyll) in a part of the Mediterranean Sea, with a focus on the influence of spatial-temporal SSH patterns on nutrient concentrations.

Methods: We downloaded monthly mean reanalysis data covering the period from 1998–2020 from the European Union Copernicus Marine Service. We applied a neural gas machine learning method to cluster SSH data and used MATLAB for data processing, anomaly calculations, spatial mapping, and exploring relationships with biological parameters.

Results: The neural gas method identified distinct interannual signals in SSH anomaly data, linking them to changes in surface and subsurface circulations in the Ionian Sea. Classification of SSH allowed for the association of SSH anomalies with varying nutrient concentrations. The analysis highlighted the role of the Adriatic-Ionian Bimodal Oscillating System in regulating SSH and nutrient patterns.

Conclusions: The neural gas method was established as a robust classification tool for detecting low-variability signals in the spatio-temporal dynamics of SSH, enabling connections with nutrient concentrations. This underscores the importance of employing nonlinear statistical methods to understand the relationship between biological and physical parameters in the Mediterranean Sea.

Keywords: Mediterranean Sea; sea surface height; neural gas; spatial temporal analysis; BiOS; European Union Copernicus Marine Service; nutrients; chlorophyll



The Ionian Sea significantly influences the Mediterranean basin's ocean circulation. The Adriatic-Ionian Bimodal Oscillating System (BiOS) drives the circulation of the Northern Ionian Gyre and modifies thermohaline shifts in water masses in the Central Mediterranean and Adriatic Sea (1). During cyclonic phases, Modified Atlantic Water follows a more direct pathway through the Sicily Channel into the central Ionian Sea and subsequently toward the Levantine Basin, facilitating enhanced vertical mixing, chlorophyll blooms, and nutrient upwelling, thereby increasing Adriatic productivity (2–5). Conversely, during anticyclonic phases of the Northern Ionian Gyre, Modified Atlantic Water is diverted northeastward along the Greek shelf, limiting its intrusion into the Adriatic, while enhancing the transport of Levantine Intermediate Water into the central Mediterranean. This promotes stratification, which reduces productivity and nutrient availability. Meanwhile, BiOS phases, with documented reversals in 1987, 1997, 2007, and 2017, demonstrate the connection between wind-driven processes, salinity, and biological productivity (4–8).

Southwest of the Peloponnese, the Pelops Gyre is a quasi-persistent mesoscale anticyclonic eddy induced by Etesian winds during summer. It modulates the westward transport of Levantine Intermediate Water, extending to depths of 800–900 meters. Seasonal variations in wind stress curl influence its intensity. The Eastern Mediterranean Transient, an extreme event that occurred between 1988 and the early 2000s, temporarily diminished the cyclonic characteristics of the Pelops Gyre (7–9).

Nutrient dynamics in the Ionian Sea are linked to reversals of the Northern Ionian Gyre, which affect circulation patterns and nutrient availability in the region. Cyclonic phases reduce nutrient availability by downwelling the nitracline to depths of 200–300 meters, while anticyclonic phases induce upwelling, increasing nutrient concentrations and supporting early winter blooms. These blooms, observed from December to January, sustain elevated productivity into March. The interaction between stable and mixed layers driven by the Northern Ionian Gyre affects nutrient distribution and biological activity across the region (3, 5, 7, 9).

In the southern Ionian Sea, the Libyan-Egyptian Current generates large mesoscale anticyclonic eddies, such as the Sirte Gyre and Messina Rise Vortex. These eddies influence the Mid-Ionian Jet, connecting the Sicily Channel with the Cretan Passage. The variability of these features modulates the inflow of Atlantic Water and Levantine Surface Water, affecting salinity, nutrient dynamics, and biological productivity. The retention properties of these gyres also trap marine particles and redistribute water masses within the Eastern Mediterranean (8, 9).

In this study, we investigate the hypothesis that variations in sea surface height (SSH) anomalies are associated with changes in nutrient concentrations. By analyzing long-term SSH anomalies and nutrient fields, we aim to explore whether specific circulation patterns reflected in SSH variability correspond to differences in ammonia, nitrate, phosphate, and chlorophyll concentrations in the Mediterranean Sea.

While the relationship between SSH anomalies and circulation patterns in the Mediterranean has been studied previously, few studies have directly analyzed how these SSH anomalies relate to nutrient concentrations using nonlinear classification methods (10, 11). Here, SSH is treated as a proxy reflecting large-scale circulation regimes, vertical



mixing, and water mass exchanges that may indirectly influence nutrient distributions. In addition to the Adriatic-Ionian BiOS, other physical processes such as mesoscale eddies, wind variability, and freshwater inputs may also contribute to the observed patterns but are beyond the scope of this analysis.

Our analysis primarily focuses on large-scale SSH patterns, with particular attention to BiOS-related variability, while recognizing that additional physical processes may also contribute to nutrient distributions.

Materials and methods

Data

This study focuses on the Mediterranean region, covering latitudes from 30.18°N to 45.98°N and longitudes from 6°W to 36.29°E. We obtained data on the SSH above the geoid from the Mediterranean Sea Physics Reanalysis (12) for the period January 1988 to December 2020. The SSH data are provided as monthly means with a horizontal resolution of $0.042^{\circ} \times 0.042^{\circ}$ (approximately 4 kilometers), giving a total of 396 monthly time steps over 33 years. We downloaded nutrient concentrations (NH₄ $^+$, NO₃ $^-$, PO₄ 3 $^-$) and chlorophyll-a as monthly mean values from the Global Ocean Biogeochemistry Analysis and Forecast dataset (13) for the period January 1998 to December 2020. These data have a horizontal resolution of 1/4° (approximately 28 km) and were analyzed at a depth of 72 m. We selected this depth after evaluating available nutrient profiles in the database, which showed that the most representative and stable measurements for ammonia, nitrate, phosphate, and chlorophyll concentrations across the upper layers were typically found between 50 and 100 meters. Therefore, 72 meters was chosen as a compromise depth within this range. Both datasets were directly retrieved from the Copernicus Marine Service (**Figure 1, Table 1**)

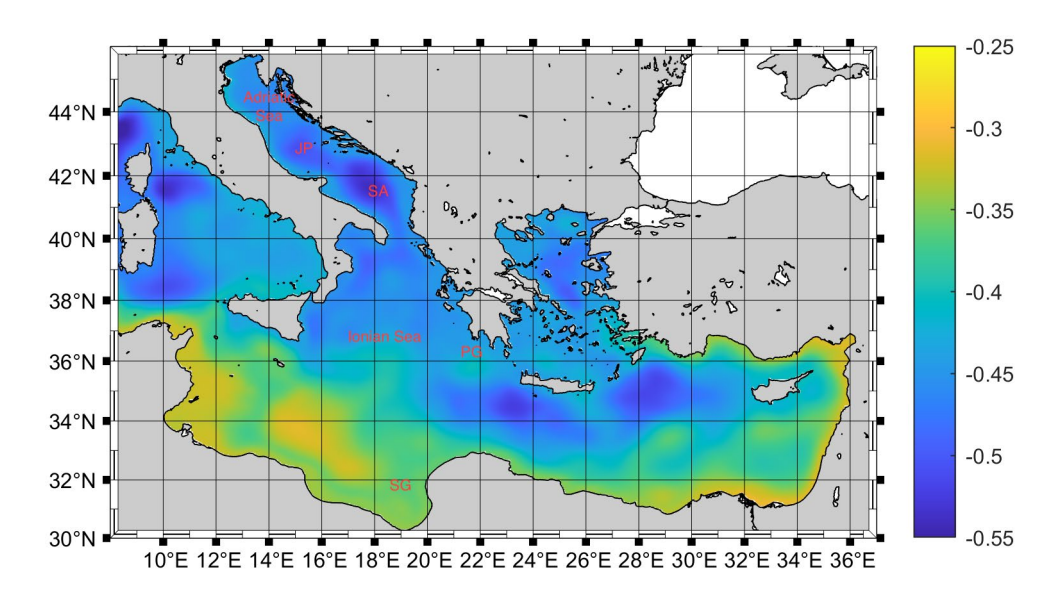


Figure 1. Mean Sea Surface Height (SSH) field in the Mediterranean Sea, calculated as the average over the period 1988–2020 from the MEDSEA_MULTIYEAR_PHY_006_004 dataset. The figure also indicates the main sub-basins and circulation features discussed in the study: Pelops Gyre (PG), Sirte Gyre (SG), Southern Adriatic Gyre (SA), Jabuka Pit (JP), Ionian Sea, and Adriatic Sea.



Table 1. The data covering the period from January 1988 to December 2020 were downloaded from two E.U. Copernicus Marine Service databases*

Variable	Latitude	Longitude	Period	Depth
Sea surface height	6°W - 36.2900°E	30.1800°N - 45.9792°S	January 1988 to December 2020	0 m
Chlorophyll mass concentration	6°W - 36.2900°E	30.1800°N - 45.9792°S	January 1999 to December 2020	72 m
Ammonia concentration	6°W - 36.2900°E	30.1800°N - 45.9792°S	January 1999 to December 2020	72 m
Nitrate concentration	6°W - 36.2900°E	30.1800°N - 45.9792°S	January 1999 to December 2020	72 m
Phosphate concentration	6°W - 36.2900°E	30.1800°N - 45.9792°S	January 1999 to December 2020	72 m

^{*}Sea surface height data were obtained from the Mediterranean Sea Physics reanalysis (10), and ocean nutrient parameters were downloaded from the Global Ocean Biogeochemistry Analysis and Forecast (11).

To remove seasonal variability, we computed anomalies by subtracting the long-term monthly climatological mean from each monthly data point. We then standardized all data using z-score normalization, where each variable was centered by subtracting its mean and scaled by its standard deviation. This ensured that all spatial fields, expressed in different units, were comparable and that the algorithm we used for analysis could process the input data effectively (10, 11).

Methods

Neural gas (NG) is a machine learning algorithm that belongs to the group of unsupervised, competitive, and self-organizing learning methods. Competitive learning is an unsupervised learning approach where neurons compete to best fit the input data, and only the neuron that best describes the input becomes the winning neuron, *i.e.*, the best-matching unit (BMU). Self-organizing learning refers to the system's ability to adjust its parameters over time based on the data it receives (14, 15).

The NG method is based on Hebb's learning rule, which states that synaptic connections between two neurons strengthen when both are active simultaneously. This rule is often summarized as: 'neurons that fire together, wire together'. The method operates by creating a network of neurons in the data space and adjusting their positions to optimally cover the entire dataset, spreading through the data like gas. It distributes neurons efficiently within the data space, taking into account the distance between neurons and the input data. The NG algorithm is used for vector quantization and consists of the following steps:

- Initialization: the neuron network is randomly positioned in the data space.
- Competition: for each input, the algorithm identifies the neuron whose position is closest to the input (BMU).
- Updating neuron positions: the BMU adjusts its position to move closer to the input data. Other neurons also adjust, but to a lesser extent, depending on their distance from the BMU.



- Decreasing adaptation: as the algorithm progresses through epochs (iterations over the full dataset), the magnitude of adaptation and the range of neurons being updated gradually decrease, allowing for more precise learning. An epoch is defined as one complete cycle during which the algorithm processes all data points once.
- Stopping: the algorithm stops after a predefined number of iterations or when adjustments become negligibly small.

Here we applied the NG model to the monthly mean SSH anomaly data. The two-dimensional spatial SSH fields were reshaped into one-dimensional vectors for each time step. We then organized the spatial vectors into an input matrix, where each row represented one month, and each column represented a spatial grid point. We set the number of neurons (BMUs) in the NG model to five based on empirical testing: we tested several neuron numbers (ranging from 3 to 10) and found that five BMUs provided a balance between capturing the main variability patterns, while avoiding overfitting and unnecessary fragmentation of the data.

We trained the NG model using SSH anomalies for the full period from January 1988 to December 2020. After classification, we used the BMU time series to analyze nutrient and chlorophyll data for the same period. Nutrient composites for each BMU were calculated only over this shorter common period, while the NG classification itself was based on the full SSH record (15).

To assess the robustness of the NG clustering, we executed the algorithm multiple times with different random initializations. The BMU assignments and resulting spatial patterns remained stable across runs, indicating that the clustering solution was robust. The final configuration used for analysis showed stable separation between BMUs and consistent identification of dominant spatial SSH patterns.

SSH anomalies may reflect circulation changes that modify vertical mixing, water mass exchange, and nutrient redistribution, thus indirectly affecting nutrient concentrations. For each BMU, we identified the corresponding months (*i.e.*, when the BMU was active) and averaged the nutrient and chlorophyll-a fields for those months at each grid point to produce composite anomaly fields. In this way, spatial distributions of nutrients and chlorophyll-a were linked to specific SSH anomaly patterns identified by the NG model.

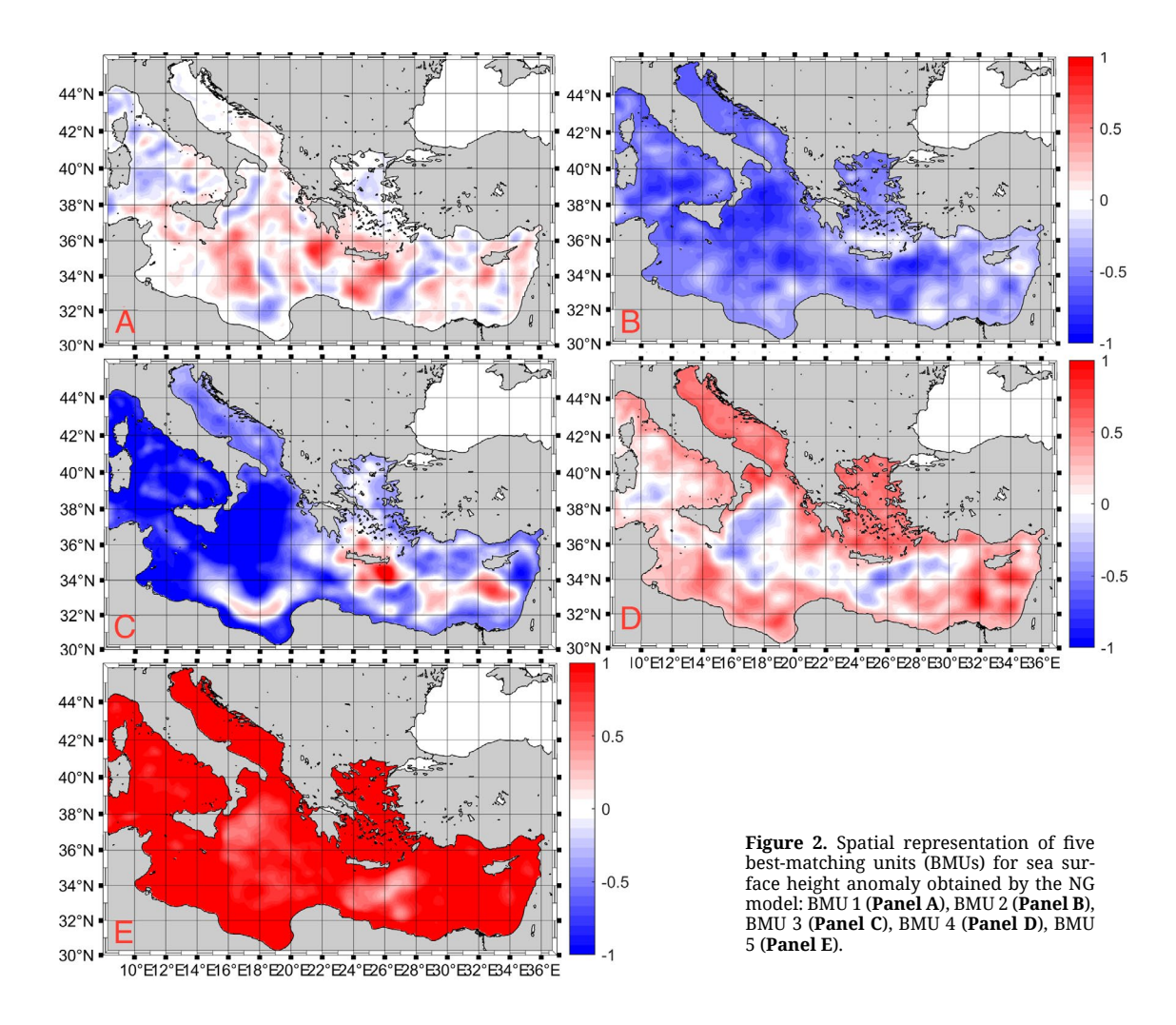
Similarly, we identified the corresponding months (*i.e.*, when that BMU was active) for each BMU based on SSH classification. We extracted the nutrient (ammonia, nitrate, phosphate) and chlorophyll-a fields for those months and averaged them at each grid point to produce composite fields. These fields represent averages of standardized anomalies (z-scores), allowing consistent comparison with SSH anomaly patterns.

We used MATLAB SOM Toolbox 2.0 (16, 17) for computing the NG.



Results

The NG analysis on sea level data highlighted five distinct BMUs (**Figure 2**). Following the initial identification of five BMUs, we examined the relationships between these units and four key variables: ammonia, nitrate, phosphate, and chlorophyll. The approach involved tracking the time points when each BMU appeared, extracting the corresponding values from the four variables at those times, and then calculating their averages across all observed time points. We repeated this step systematically for all BMUs, providing insights into how these variables interact over time.



BMU 1 shows scattered positive and negative anomalies across the Mediterranean, with a prominent positive anomaly south of the Peloponnese, suggesting a vortex. BMU 2 depicts the entire Mediterranean as a negative anomaly, in contrast to BMU 5, which shows a positive anomaly across the region. BMU 3 primarily displays negative anomalies in the Adriatic, except near the Tunisian coast, where a slight positive anomaly is observed. This positive SSH anomaly may result from anticyclonic BiOS phases, during which the northward advection of warm, saline Levantine water enhances steric sea level in the southern Adriatic and Tunisian shelf region. Positive anomalies are also evident south of Greece



and in the Eastern Mediterranean. BMU 4 reflects a significant negative sea level anomaly in the Ionian Sea, characteristic of a cyclonic vortex associated with BiOS oscillation. The Adriatic shows predominantly negative anomalies in BMU 2 and BMU 3, while it is markedly positive in BMU 4 and BMU 5.

The time series covering the period from 1998 to 2020 for BMU is shown in Figure 3. Transitions between different BMUs are rare, as BMUs remain persistent over time. The BMU3 neuron appears at the beginning of the time series and remains active without transitions for almost three years. This period is defined as the first oscillation regime (OR), i.e., (OR3) because it represents the initial stable circulation pattern detected at the start of the analyzed period. We identified two distinct oscillation regimes: OR3, dominated by BMU3, and the dominant regime OR245, characterized by alternating occurrences of BMU2, BMU4, and BMU5 throughout the remaining time series. The behavior of OR245 changed during the analyzed period, with the most frequent BMU in OR245 varying over time. BMU2 was dominant between 2001-2004 and 2015-2019, while BMU4 was the most frequent between 2008-2015. The temporary appearance of BMU1 between 2004 and 2007 may reflect a short-term deviation in the circulation system, possibly linked to changes in wind forcing, freshwater input, or mesoscale activity that temporarily modified the largescale Ionian circulation. However, due to the limited duration and isolated occurrence of BMU1, this period is not defined as a separate third oscillation regime but rather as a transient disruption within the dominant OR245 regime.

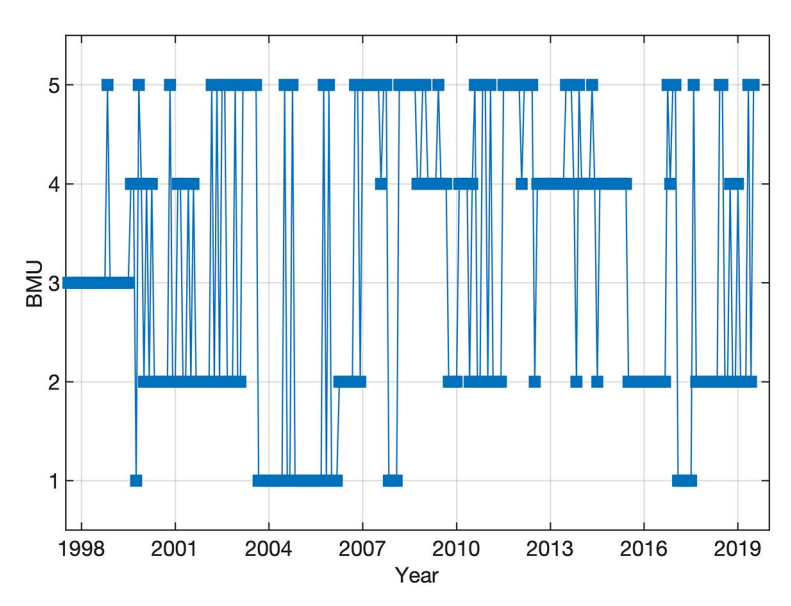


Figure 3. Temporal evolution of the winning neurons (best-matching units, BMUs) obtained from the NG model using SSH anomaly data.



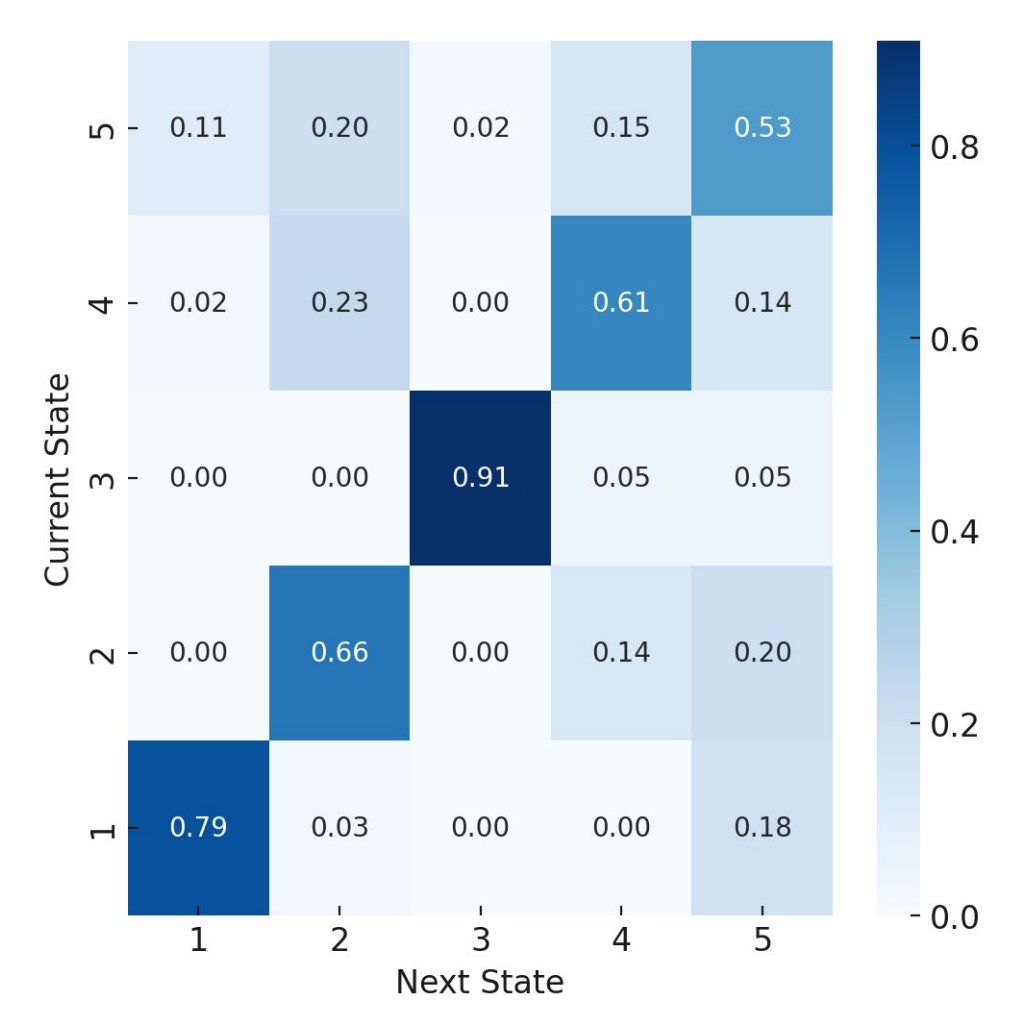
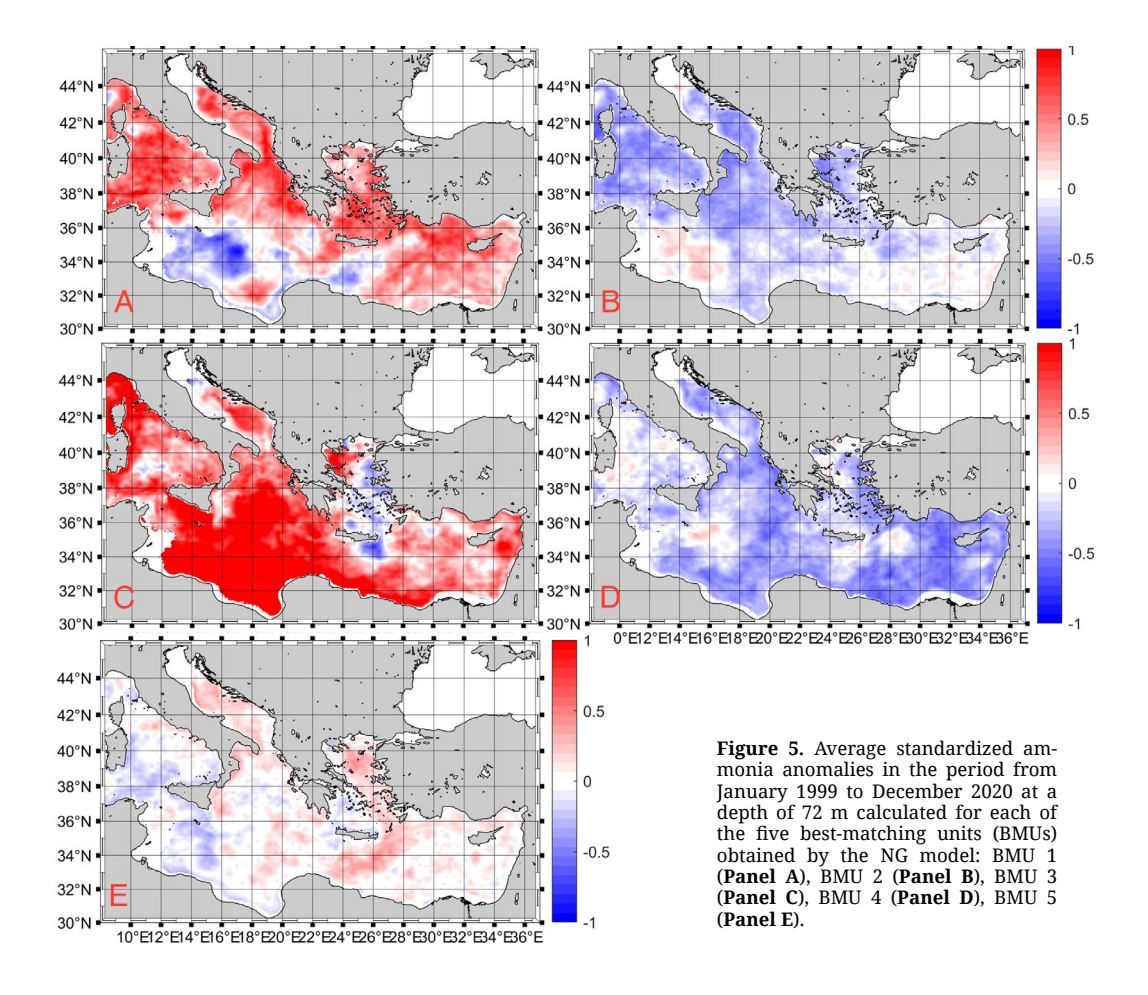


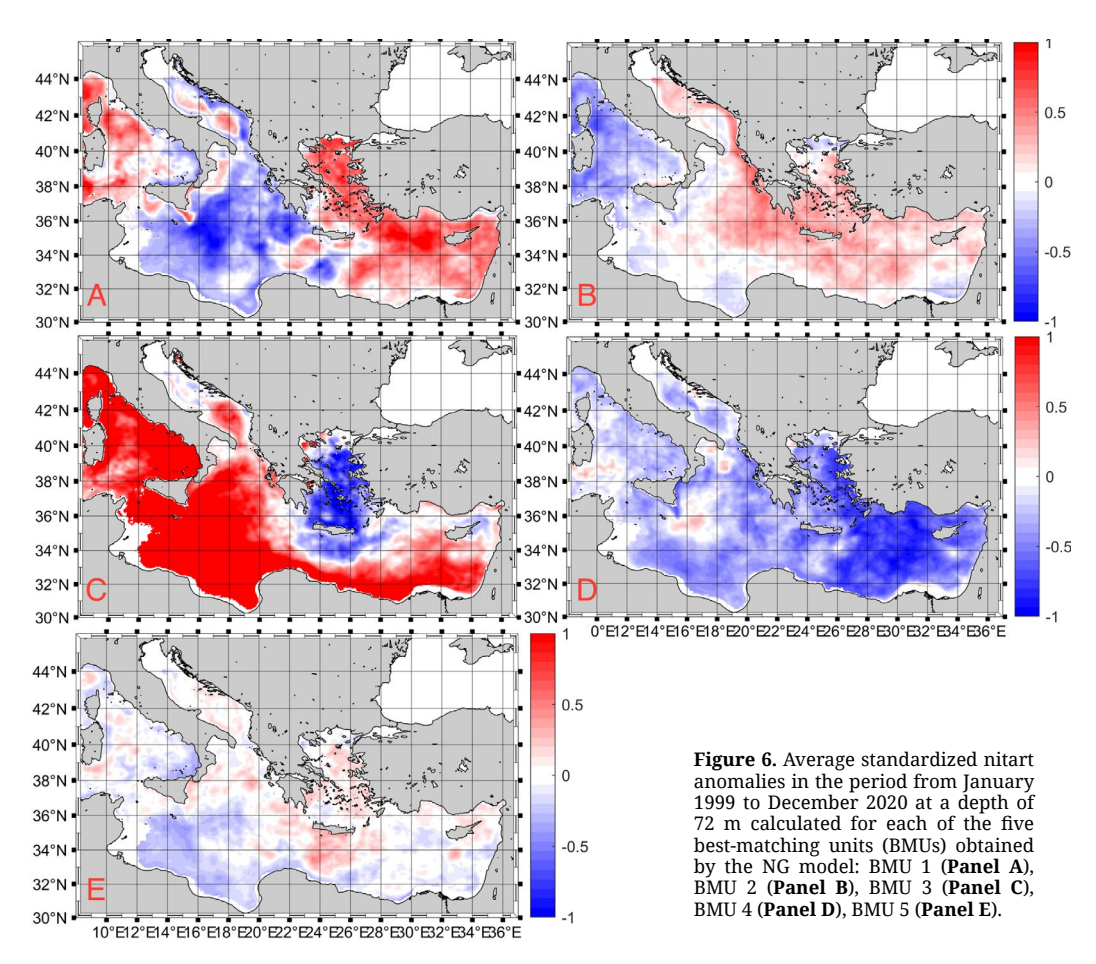
Figure 4. Markov Chain Transition Matrix for best-matching units (BMU).

The persistence of the dominant neuron in different oscillation systems is shown in **Figure 4**, which presents a matrix of transition probabilities between neurons. BMU3 is the most stable, with a 91% probability of remaining in the same state. In contrast, BMU5 is the most variable, with a 49% probability of switching to a different neuron.

Once we successfully trained the NG model, we used it to analyze the relationship between nutrients, chlorophyll, and the identified BMUs.

For ammonia, BMU 1 and BMU 3 indicate high concentrations (positive anomalies), while BMU 2 and BMU 4 show low concentrations (negative anomalies) (**Figure 5**). BMU 5 reflects a neutral state. BMU 1 displays positive anomalies in the northern part of the Mediterranean, while negative anomalies are observed in the southern part. Additionally, a positive circular pattern is noted near northern Libya. In BMU 2, the northern region exhibits slightly negative anomalies, whereas the southern region shows localized weak positive anomalies. This reflects an inverted situation compared to BMU 1. Irregular anomalies are mostly seen on BMU 3. Primarily positive across much of the Mediterranean, with exceptions found in the Aegean Sea. A circular structure, or vortex, is also present around Crete. A positive anomaly is observed in the northern Adriatic and between the islands of Sardinia and Sicily. Similar to BMU 2, BMU 4 shows that almost the entire Mediterranean exhibits negative anomalies, except for the area south of Sicily, where slightly positive

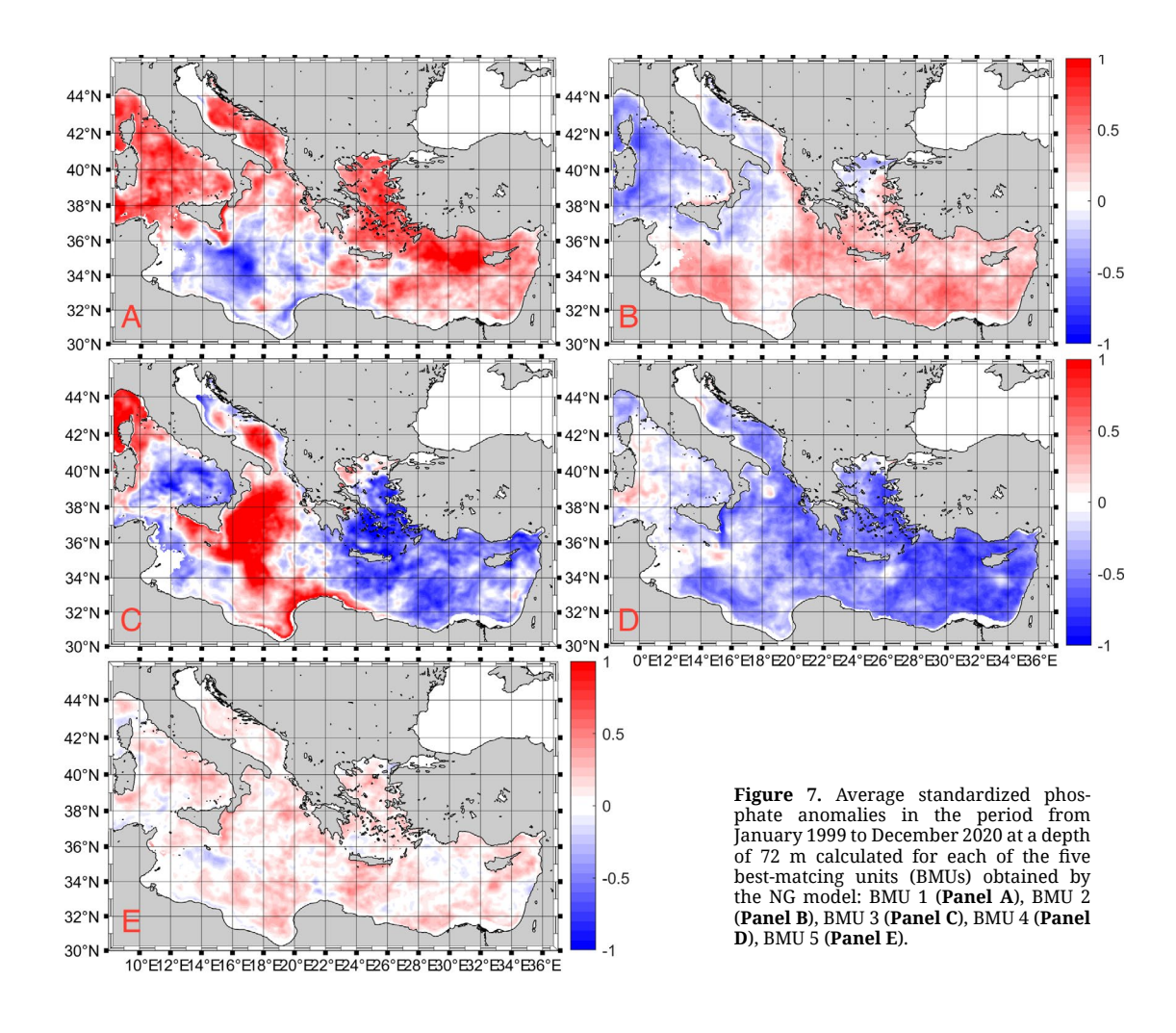






anomalies are present. BMU 5 exhibits very small anomalies; however, it predominantly contains positive anomalies that are spatially uneven. The Adriatic and Aegean Seas are slightly positive, while the western Mediterranean and areas south of Sicily are negative.

Figure 6 shows the dissolved nitrate anomaly fields obtained from the NG model. BMU 1 exhibits a pronounced anomaly in the southern Adriatic, where a clear difference between northern and southern parts of the basin can be seen. This structure may be related to circulation features influencing the nitrate distribution in this region. Other localized features are also visible, for example, off the east coast of Crete. The Adriatic does not behave as a uniform body, but rather shows strong spatial variability. The Ionian Sea indicates circulation patterns suggestive of BiOS activity, while most of the Mediterranean displays positive anomalies. A significant negative anomaly is observed in the Aegean Sea, whereas the remainder of the Mediterranean shows generally positive anomalies. In BMU 2, there is a clear extension of positive anomalies into the Adriatic Sea from the Ionian, with positive values along the Greek coast and negative values along the Italian coast. BMU 3 shows an opposite pattern compared to BMU 1, with widespread positive anomalies over most of the Mediterranean except for negative anomalies in the Aegean Sea. A weak circular structure is visible south of Crete, while no significant anomalies are present in the northern Adriatic or between Sardinia and Sicily in this BMU. BMU 4 shows predominantly negative anomalies across the Mediterranean, without clear similarity to



BMU 2. We avoid using the word "trend" here, as the anomalies represent spatial distributions rather than temporal tendencies. BMU 5 is characterized by near-neutral anomalies, with small positive anomalies in the Adriatic and Aegean Seas and negative anomalies in the western Mediterranean and south of Sicily. Along the African coast, weak spatial variability is observed, while south of Crete a more distinct negative anomaly appears, which may indicate local circulation effects.

Figure 7 illustrates the dissolved phosphate anomaly fields presented for the five BMUs. The analysis reveals spatial variability in the Adriatic and surrounding seas. In BMU 1, positive anomalies are present along both the Greek and Italian coasts, extending into the Adriatic and reaching toward Sicily. This suggests a more widespread enrichment pattern affecting the entire entrance of the Adriatic. BMU 2 shows positive anomalies along the coasts of Greece and Albania, while negative anomalies appear in the central and western parts of the Adriatic, indicating regional differences within the basin. In BMU 3, positive anomalies dominate the South Adriatic and Jabuka basins, while localized negative anomalies are observed along parts of the Croatian coast and north of Jabuka. BMU 4 exhibits predominantly negative anomalies across the Mediterranean, indicating lower phosphate concentrations during this regime. BMU 5 displays generally weak anomalies, with slight positive values in parts of the Adriatic and Ionian Seas, suggesting a mildly elevated phosphate concentration compared to other BMUs.

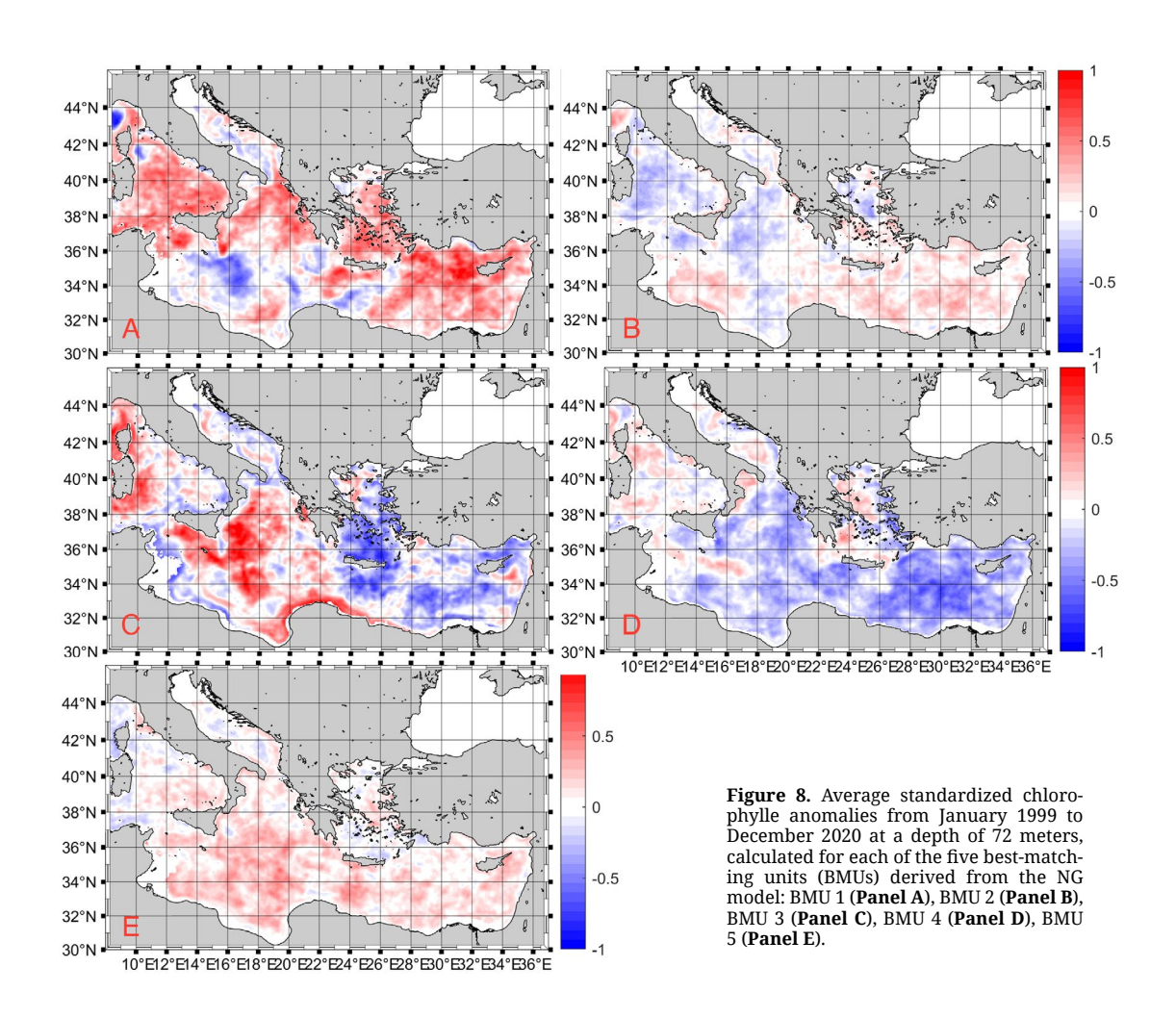




Figure 8 presents the chlorophyll anomaly fields obtained for the five BMUs. On average, chlorophyll anomalies are generally low across the Mediterranean. In the Adriatic Sea, anomalies are weak, while more pronounced anomalies are visible in parts of the eastern Mediterranean. BMU 1 shows generally positive anomalies, with positive values extending from the Ionian Sea into the Adriatic along the Greek coast, while slightly lower values are present along the Italian coast. In BMU 2, approximately half of the Mediterranean displays weak negative anomalies, while the remaining areas, particularly in the eastern Mediterranean, exhibit weak positive anomalies.BMU 3 displays generally positive anomalies, with a stronger positive signal in the Ionian Sea. BMU 4 shows weak negative anomalies across most of the Mediterranean, including the Adriatic. Compared to BMU 4, BMU 5 exhibits slightly more positive anomalies in many regions; however, both BMUs show similar patterns in the eastern Mediterranean, where positive anomalies dominate.

Although BiOS represents the dominant large-scale mechanism in this region, other physical drivers such as mesoscale eddies, wind stress variability, and freshwater fluxes may also contribute to nutrient distribution. Similar approaches relating SSH anomalies and nutrient variability have been reported in previous studies (1, 3), supporting the relevance of this analysis.

The presence of vortex-like structures in the nutrient fields (*e.g.*, in the southern Adriatic) that are not always clearly visible in SSH anomalies may reflect differences in the physical and biogeochemical response times. Nutrient distributions are influenced by the cumulative effect of physical transport, biological uptake, and residence times, which may allow weaker or more persistent circulation features to emerge more clearly in the nutrient composites than in the more transient SSH anomaly fields.

Discussion

This study identified significant spatiotemporal changes in sea level and nutrient concentrations in the Mediterranean Sea over the analyzed period (1998–2020). The application of the NG algorithm allowed for the classification of sea surface height (SSH) anomalies and their association with variations in ammonia, nitrate, phosphate, and chlorophyll concentrations.

The persistence of BMUs observed in the NG time series reflects relatively stable large-scale circulation regimes, consistent with the known multi-year variability of processes such as the Adriatic-Ionian BiOS and broader decadal oscillations in the Ionian Sea. However, it should be noted that the NG algorithm, by its design, also favors stable classification once neurons are well-separated, especially when large-scale low-frequency processes dominate the variability. Therefore, part of the BMU persistence likely reflects both physical stability and the inherent behavior of the clustering method.

The stability of these regimes suggests persistent oceanic processes governing SSH, which consequently influence nutrient concentrations through mechanisms such as water mass exchange, vertical mixing, and horizontal advection. The BiOS appears to be one of the im-



portant contributors modulating SSH variability, particularly as reflected in BMU4, which corresponds to the cyclonic BiOS phase that is typically associated with enhanced vertical mixing. However, in the analyzed data, this mixing did not always correspond to elevated nutrient concentrations, as negative anomalies in ammonia were observed for BMU4. This suggests that additional factors such as prior nutrient depletion, stratification history, or circulation pathways may also strongly affect nutrient availability under different SSH regimes.

The persistence of BMU3, with a 91% probability of remaining in the same state, indicates a highly stable circulation regime, while BMU5 exhibited the highest variability, reflecting more frequent transitions between different SSH patterns. Nutrient concentrations showed distinct differences across BMUs, with BMU1 and BMU3 generally associated with higher ammonia levels, while BMU2 and BMU4 were characterized by lower nutrient concentrations (11).

The obtained SSH and nutrient patterns are broadly consistent with previous studies describing circulation and biogeochemical variability in the Adriatic-Ionian system (1, 3). However, SSH anomalies likely reflect a superposition of multiple physical mechanisms, including BiOS variability, mesoscale eddies, wind stress variability, and exchanges with neighboring basins. These combined processes contribute to the observed nutrient patterns, which cannot be attributed solely to SSH anomalies (7, 9).

The observed chlorophyll patterns suggest only weak biological responses to SSH anomalies, with minimal deviations across BMUs. This may indicate that additional factors such as light availability, stratification strength, grazing pressure, or nutrient limitation influence phytoplankton productivity more directly than SSH-related processes alone.

We tested the NG clustering results for robustness by executing multiple runs with different initializations, which produced stable BMU assignments and consistent spatial patterns. This supports the reliability of the clustering solution, although some simplification of complex variability remains inherent in the statistical reduction of the data.

Finally, the presence of vortex-like structures in the nutrient fields (*e.g.*, in the southern Adriatic) that are not always clearly seen in SSH anomalies may reflect the longer residence times and cumulative effects of physical and biological processes in nutrient distributions, allowing such features to emerge more distinctly in nutrient fields than in SSH patterns.

The NG algorithm successfully identified spatio-temporal SSH regimes and their association with nutrient distributions in the Mediterranean Sea. Our results demonstrate that SSH anomalies correspond to distinct nutrient patterns and suggest that circulation-driven processes contribute to nutrient redistribution. The BiOS likely plays an important, but not exclusive, role in modulating these patterns. Lastly, our approach highlights the potential of nonlinear classification methods such as NG for detecting low-variability signals and investigating physical-biogeochemical interactions.



Provenance: Submitted. This manuscript is based on the master's thesis by Ivona Siber, deposited in the Dabar repository (https://urn.nsk.hr/urn:nbn:hr:172:703297).

Received: 30 January 2025 / Accepted: 16 July 2025 / Published online: 6 November 2025.

Peer review: Externally peer reviewed.

Data availability: The data used for the purpose of this research are available *via* the databases cited in the "Methods" section of the manuscript.

Ethical approval: Not required.

Funding: The authors received no financial support for the research, authorship, or publication of this article.

Authorship declaration: Both authors contributed equally to the work and approved the final version of the manuscript. They take full accountability for the work.

Disclosure of interest: The authors completed the ICMJE Disclosure of Interest Form (available upon request from the corresponding author) and disclose no relevant interests.

ORCID

Ivona Siber https://orcid.org/0009-0008-8997-3779

Frano Matić (b) https://orcid.org/0000-0003-0392-4172

References

- 1. Gačić M, Borzelli GE, Civitarese G, Cardin V, Yari S. Can internal processes sustain reversals of the ocean upper circulation? The Ionian Sea example. Geophys Res Lett. 2010;37(9):100. https://doi.org/10.1029/2010GL043216
- 2. Gačić M, Schroeder K, Civitarese G, Cosoli S, Vetrano A, Eusebi Borzelli GL. Salinity in the Sicily Channel corroborates the role of the Adriatic–Ionian Bimodal Oscillating System (BiOS) in shaping the decadal variability of the Mediterranean overturning circulation. Ocean Sci. 2013;9:83–90. https://doi.org/10.5194/os-9-83-2013
- 3. Civitarese G, Gačić M, Batistić M, Bensi M, Cardin V, Dulčić J, et al. The BiOS mechanism: History, theory, implications. Prog Oceanogr. 2023;216:103056. https://doi.org/10.1016/j.pocean.2023.103056
- 4. Eusebi Borzelli GL, Carniel S. A reconciling vision of the Adriatic-Ionian Bimodal Oscillating System. Sci Rep. 2023;13:2334. https://doi.org/10.1038/s41598-023-29162-2
- 5. Civitarese G, Gačić M, Lipizer M, Eusebi Borzelli GL. On the impact of the Bimodal Oscillating System (BiOS) on the biogeochemistry and biology of the Adriatic and Ionian Seas (Eastern Mediterranean). Biogeosciences. 2010;7:3987–97. https://doi.org/10.5194/bg-7-3987-2010
- 6. Meli M. The potential recording of North Ionian Gyre's reversals as a decadal signal in sea level during the instrumental period. Sci Rep. 2024;14:4907. https://doi.org/10.1038/s41598-024-55579-4
- 7. Tanhua T, Hainbucher D, Schroder K, Cardin V, Alvarez M, Civitarese G. The Mediterranean Sea system: a review and an introduction to the special issue. Ocean Sci Discuss. 2013;10:581–617. https://doi.org/10.5194/os-9-789-2013
- 8. Incarbona A, Martrat B, Mortyn PG, Sprovieri M, Ziveri P, Gogou A, et al. Mediterranean circulation perturbations over the last five centuries: Relevance to past Eastern Mediterranean Transient-type events. Sci Rep. 2016;6:29623. https://doi.org/10.1038/srep29623
- 9. Malanotte-Rizzoli P, Artale V, Borzelli-Eusebi GL, Brenner S, Crise A, Gačić M, et al. Physical forcing and physical/biochemical variability of the Mediterranean Sea: a review of unresolved



- issues and directions for future research. Ocean Sci. 2014;10:281–322. https://doi.org/10.5194/os-10-281-2014
- 10. Escudier R, Clementi E, Omar M, Cipollone A, Pistoia J, Aydogdu A, Drudi M, Grandi A, Lyubartsev V, Lecci R, et al. Mediterranean Sea Physical Reanalysis (CMEMS MED-Currents) (Version 1) [Data set]. 2020.
- 11. Cossarini G, Feudale L, Teruzzi A, Bolzon G, Coidessa G, Solidoro C, et al. High-resolution reanalysis of the Mediterranean Sea biogeochemistry (1999-2019). Front Mar Sci. 2021;8:741486. https://doi.org/10.3389/fmars.2021.741486
- 12. Mediterranean Sea Physics Reanalysis. Copernicus. 2025 [cited 2025 Aug 18]. Available from: https://doi.org/10.25423/CMCC/MEDSEA MULTIYEAR PHY 006 004 E3R1.
- 13. Mediterranean Sea Biogeochemistry Reanalysis. Copernicus. 2025 [cited 2025 Aug 18]. Available from: https://doi.org/https://doi.org/10.25423/cmcc/medsea_multiyear_bgc_006_008_medbfm3.
- 14. Hebb DO. The Organization of Behavior: A Neuropsychological Theory. London (UK): John Wiley & Sons, Inc.; 1949.
- 15. Kohonen T. Self-Organizing Maps, third edition. Heidelberg (Germany): Springer Berlin; 1995.
- 16. Toolbox SOM. 2015 Feb 3 [cited 2025 Aug 18]. Available from: http://www.cis.hut.fi/somtoolbox.
- 17. Martinetz TM, Berkovich SG, Schulten KJ. Neural-Gas Network for vector quantization and its application to time-series prediction. IEEE Trans Neural Netw. 1993;4(4):558–69. https://doi.org/10.1109/72.238311

